CRYSTALLOGRAPHIC TEXTURES OF HOT ROLLED STEELS

Dierk Raabe

Max-Planck-Institut für Eisenforschung
Max-Planck-Str. 1
40237 Düsseldorf
Germany
(raabe@mpie.de)

keywords: texture, stainless steel, microstructure, recrystallization, ferritic, austenitic

ABSTRACT

The present study gives a review on basic types of crystallographic textures developing during hot rolling of polycrystalline steels. The results are grouped into three fundamental classes of textures. The first group comprises pure Fe, some weakly bonded B2 and $D0_3$ structured intermetallics, as well as closely related alloys such as ferritic low carbon and microalloyed interstitial free steels. The second group includes highly alloyed corrosion-resistant ferritic stainless and Fe-Si transformer steels. Typical examples are steels with about 10 wt.%-17 wt.% Cr, with about 3 wt.% Si, as well as body centered cubic transition metals such as Ta, Mo, and Nb which do not undergo a phase transformation during hot rolling. The third group comprises stable and instable austenitic stainless steels for instance on the basis of larger amounts of Cr and Ni or on Mn as well as duplex stainless steels. Most $L1_2$ structured intermetallic alloys can also be assigned to this group. The suggested classification scheme is discussed in terms of different processing parameters, thermodynamics, microstructure, and crystallographic aspects.

ZUSAMMENFASSUNG

Diese Studie gibt einen Überblick über die wesentlichen Typen kristallograpischer Texturen von warmgewalzten polykristallinen Stählen. Die Ergebnisse lassen sich in drei fundamentale Texturklassen einteilen. Die erste Gruppe umfaßt reines Fe, einige schwach gebundene B2 und $D0_3$ strukturierte Intermetallische Phasen und eng verwandte Legierungen sowie ferritische niedriggekohlte und mikrolegierte IF Stähle. Die zweite Gruppe umfaßt hochlegierte korrosionsbeständige ferritische Edelstähle und Fe-Si Transformatorstähle. Typische Beispiele sind Stähle mit etwa 10 wt.%-17 wt.% Cr, mit etwa 3 wt.% Si sowie kubisch-raumzentrierte Übergangsmetalle wie Ta, Mo und Nb die keine Phasenumwandlung während der Warmumformung durchlaufen. Die dritte Gruppe umfaßt stabile und instabile austenitische Edelstähle zum Beispiel auf der Basis von größeren Legierungsanteilen an Cr und Ni oder Mn sowie Duplex-Edelstähle. Zahlreiche $L1_2$ strukturierte Intermetallische Legierungen können dieser Gruppe ebenfalls zugeordnet werden. Das vorgeschlagene Klassifizierungsschema wird im Hinblick auf unterschiedliche Herstellbedingungen, Thermodynamik, Mikrostrukturen und kristallographische Aspekte diskutiert.

1 Introduction

The application of quantitative texture analysis in terms of the orientation distribution function (ODF) [1,2] to a large variety of steel hot bands has during the last two decades provided a rather complete picture on the evolution of hot rolling textures of body centered cubic (BCC) and face centered cubic (FCC) steels and related alloys. The use of the ODF provides texture data for hot rolled steels which are sufficiently detailed to reveal characteristic differences between the various groups of steels. The main parameters leading to different classes of hot band steel textures can be arranged in four groups, Table 1.

Main groups of influence parameters on hot band steel textures	**Main factors in each parameter group**
group 1 (processing)	• casting conditions (e.g. continuous casting, thin strip casting) • slab treatment (e.g. slab annealing temperature, soaking time) • pre-rolling • hot rolling schedule (e.g. ferritic rolling, austenitic rolling, reduction scheme, macroscopic through-thickness strain rate profiles)
group 2 (thermodynamics)	• amount and kind of alloying elements • impurities • stored deformation energy • transformation behavior • stacking fault energy (austenite)
group 3 (microstructure)	• grain size and shape • recrystallization temperature and time • shear banding • precipitations
group 4 (crystallography)	• active slip systems • inherited textures • orientation relationships during transformation (e.g. Bain or Nishiyama-Wassermann)

Table 1: Main parameters which lead to different classes of hot band steel textures [3-12].

The first group includes the processing parameters, such as casting (e.g. continuous casting, thin strip casting), slab treatment (e.g. slab annealing temperature, soaking time), pre-rolling, and hot rolling schedule (e.g. ferritic rolling, austenitic rolling, reduction scheme, macroscopic through-thickness strain rate profiles). The second group includes thermodynamic quantities such as the amount and kind of alloying elements, impurities, transformation behavior, stored deformation energy, and the stacking fault energy of the austenitic phase. The third group comprises microstructural parameters such as the grain size and shape, recrystallization temperature and time, shear bands, and precipitations. The fourth group contains crystallographic aspects such as the active slip systems in the different phases, inherited textures, and orientation relationships during transformation (e.g. Bain or Nishiyama-Wassermann).

The texture results presented in this overview for a number of different types of hot rolled steels suggests to establish three basic classes of hot band steel textures. The first group (in the following termed group A) comprises pure Fe, some weakly bonded B2 and $D0_3$ structured intermetallics, as well as the closely related ferritic low carbon and interstitial free (IF) steels. The second group (in the following termed group B) includes highly alloyed ferritic stainless and Si-steels, particularly steels with about 10 wt.%-17 wt.% Cr or with about 3 wt.% Si as well as BCC transition metals such as Ta, Mo, Cr, and Nb which do not undergo a phase transformation during hot rolling. The third group (in the following termed group C) comprises stable and instable austenitic stainless steels for instance on the basis of larger amounts of Cr and Ni or on Mn as well as duplex stainless steels. Most $L1_2$ structured intermetallic alloys can also be assigned to this group.

Earlier reviews on the main elements of the crystallographic textures of hot rolled steels were published by Wassermann and Grewen [3], Hölscher et al. [4,5], Ray and Jonas [6], and Raabe et al. [7-13].

2 Experimental

As examples for the different groups of hot rolled steels the current report reviews data for IF deep drawing steels, various highly alloyed microalloyed and non-microalloyed corrosion-resistant ferritic stainless high grade steels with a Cr content between 10 wt.% and 17 wt.% as well as different Cr-Ni-base austenitic stainless steels. All inspected samples were industrially hot rolled to a thickness between 3-4mm.

Since textures and microstructures of hot rolled steels are often very inhomogeneous through the thickness, all specimens were measured in various through thickness layers. Some hot band textures with strong nonhomogeneity were even characterized in eleven-through-thickness layers. The inspected layer is described by the parameter $s=a/(d/2)$ with a being the distance of the actual layer from the center layer and d the sample thickness, i.e. s=0 corresponds to the center and s=1 to the surface layer. The mid-thickness layers at s=0 as well as the layers at s=0.7 and s=0.8 are particularly relevant for hot band texture analysis since they typically show the strongest plane-strain textures (s=0) and shear textures (s=0.7, s=0.8) during industrial hot rolling, respectively.

In order to remove a surface layer of 20 µm, that is to get rid of disturbing grinding effects before the texture measurements, the austenitic stainless steel samples were etched in a solution of 100 ml H_2O, 100 ml HCl and 30 ml HNO_3 at ambient temperature. The ferritic stainless steel samples were etched in a solution of 100 ml H_2O_2, 10 ml HF, 5 ml HNO_3 and 5 ml HCl. The IF steels were etched by using HF prior to the texture measurements.

All textures have been quantitatively examined by measuring four incomplete pole figures from an area of 14×24 mm^2 in the range of the pole distance angle α from 5° to 85° with $Mo_{K\alpha 1}$-radiation in the back reflection mode [14] using automatic texture goniometers and by deriving from them the ODF, f(g), by applying an iterative non-negative series expansion method [15-17] using a maximum series expansion degree of l_{max}=22. The orientation g is given in terms of three Euler angles using Bunge`s notation, φ_1, ϕ, φ_2.

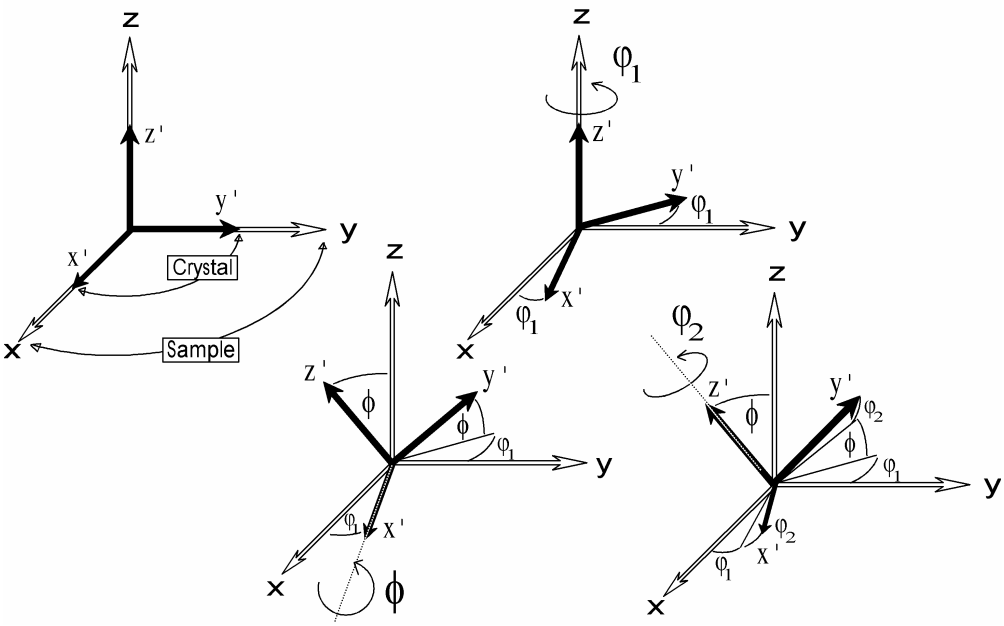

Figure 1: Definition of the three Euler angles φ_1, ϕ, φ_2 in Bunge`s notation [1,2]

3 Presentation of hot rolling textures of steels

According to the cubic crystal symmetry of both, the FCC and BCC crystal lattice and the orthothropic symmetry of the hot rolled specimens with RD = rolling direction, ND = normal direction, and TD = transverse direction of the sheets the textures are typically presented in the reduced Euler space ($0° \leq \varphi_1, \phi, \varphi_2 \leq 90°$). Since both, FCC and BCC steels tend to develop pronounced texture fibers during cold rolling, it is convenient to apply φ_1-sections in case of BCC steels and φ_2-sections in case of FCC steels through Euler space or to present the orientation density along various characteristic orientation fibers.

For BCC steels these are the α_{bcc}–fiber (fiber axis <110> parallel to the rolling direction including major components {001}<110>, {11̲2}<110>, and {11̲1}<110>), γ–fiber (fiber axis <111> parallel to the normal direction including major components {111}<110> and {11̲1}<112>), η-fiber (fiber axis <001> parallel to the rolling direction including major components {001}<100> and {011}<100>), ζ–fiber (fiber axis <011> parallel to the normal

direction including major components {011}<100>, {0$\underline{1}$1}<211>, {0$\underline{1}$1}<111>, and {0$\underline{1}$1}<011>), ε–fiber (fiber axis <011> parallel to the transverse direction including major components {001}<110>, {112}<111>, {111}<112>, and {011}<100>), and θ–fiber (fiber axis <001> parallel to the normal direction including major components {001}<100> and {001}<110>). For FCC steels these are the α_{fcc}–fiber (fiber axis <011> parallel to the normal direction including major components {011}<100>, {0$\underline{1}$1}<211>, {0$\underline{1}$1}<111>, and {0$\underline{1}$1}<011>) and the β–skeleton line (less symmetric fiber including major components {211}<111> (Cu–component), ~{123}<634> (S–component) and {011}<211> (Brass–component)).

The most important orientations and fibers are also given in Figures 1a,b and Table 2. While some texture fibers depict the intensities of the orientations at fixed Euler angles, the β-skeleton line is not a static fiber, but collects the local maxima with varying coordinates in Euler space.

Material	Fiber name	Fiber axis	Important components
BCC phase	α_{bcc}–fiber	<110> parallel to RD	{001}<110>, {1$\underline{1}$2}<110>, {1$\underline{1}$1}<110>
	γ–fiber	<111> parallel to ND	{111}<110>, {11$\underline{1}$}<112>
	η–fiber	<001> parallel to RD	{001}<100>, {011}<100>
	ζ–fiber	<011> parallel to ND	{011}<100>, {0$\underline{1}$1}<211>, {0$\underline{1}$1}<111>, {0$\underline{1}$1}<011>
	ε–fiber	<011> parallel to TD	{001}<110>, {112}<111> {4 4 11}<11 11 8>, {111}<112>, {11 11 8}<4 4 11>, {011}<100>
	θ–fiber	<001> parallel to ND	{001}<100>, {001}<110>
	β_{bcc}–skeleton line	≈ <111> close to ND	{111}<110>, {557}<583>, {111}<112>
FCC phase	α_{fcc}–fiber	<011> parallel to ND	{011}<100>, {0$\underline{1}$1}<211>, {0$\underline{1}$1}<111>, {0$\underline{1}$1}<011>
	β_{fcc}–skeleton line	less symmetric fiber following local texture maxima rather than fixed coordinates	{211}<111>, {123}<634>, {011}<211>

Table 2: Some important fibers and texture components for BCC and FCC steels.

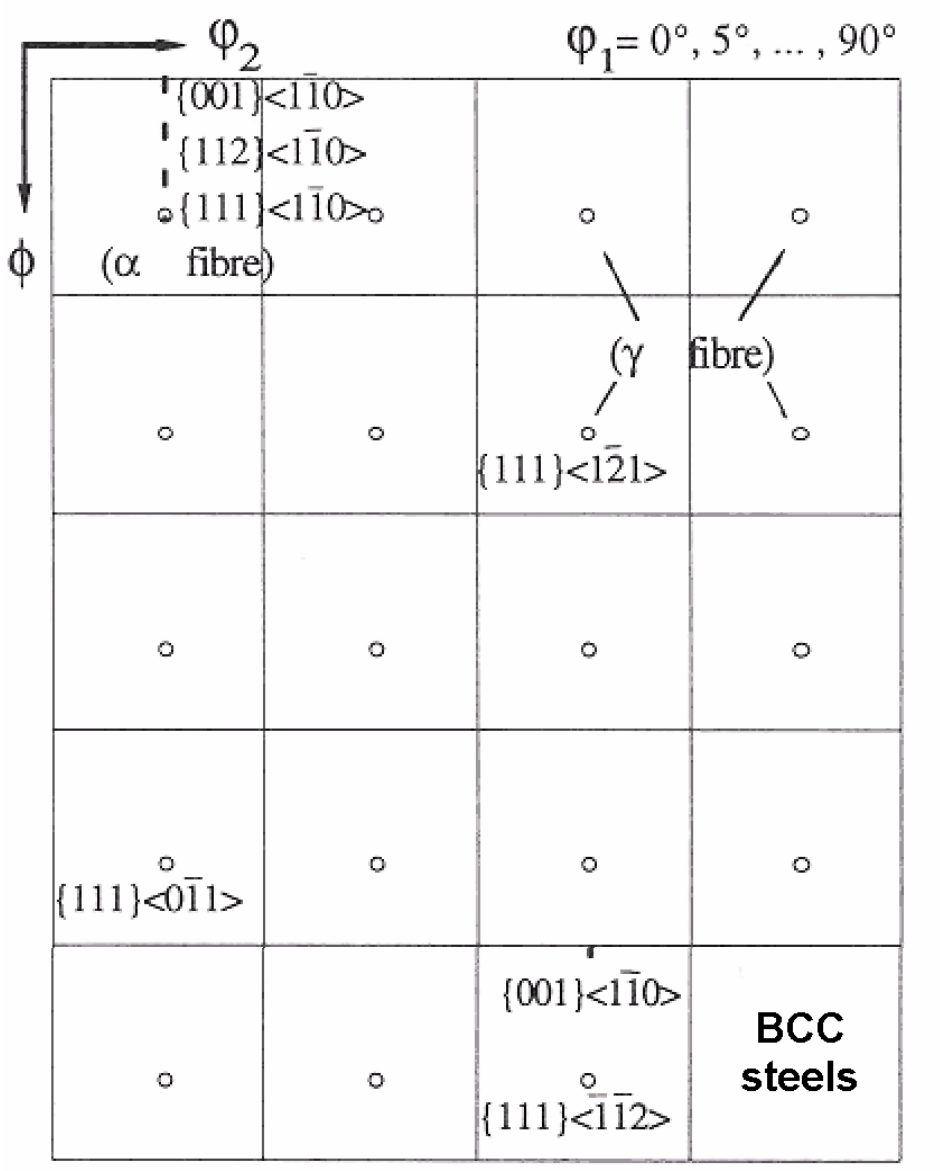

Figure 2: Some important fibers and texture components for BCC steels in sections through the reduced Euler space.

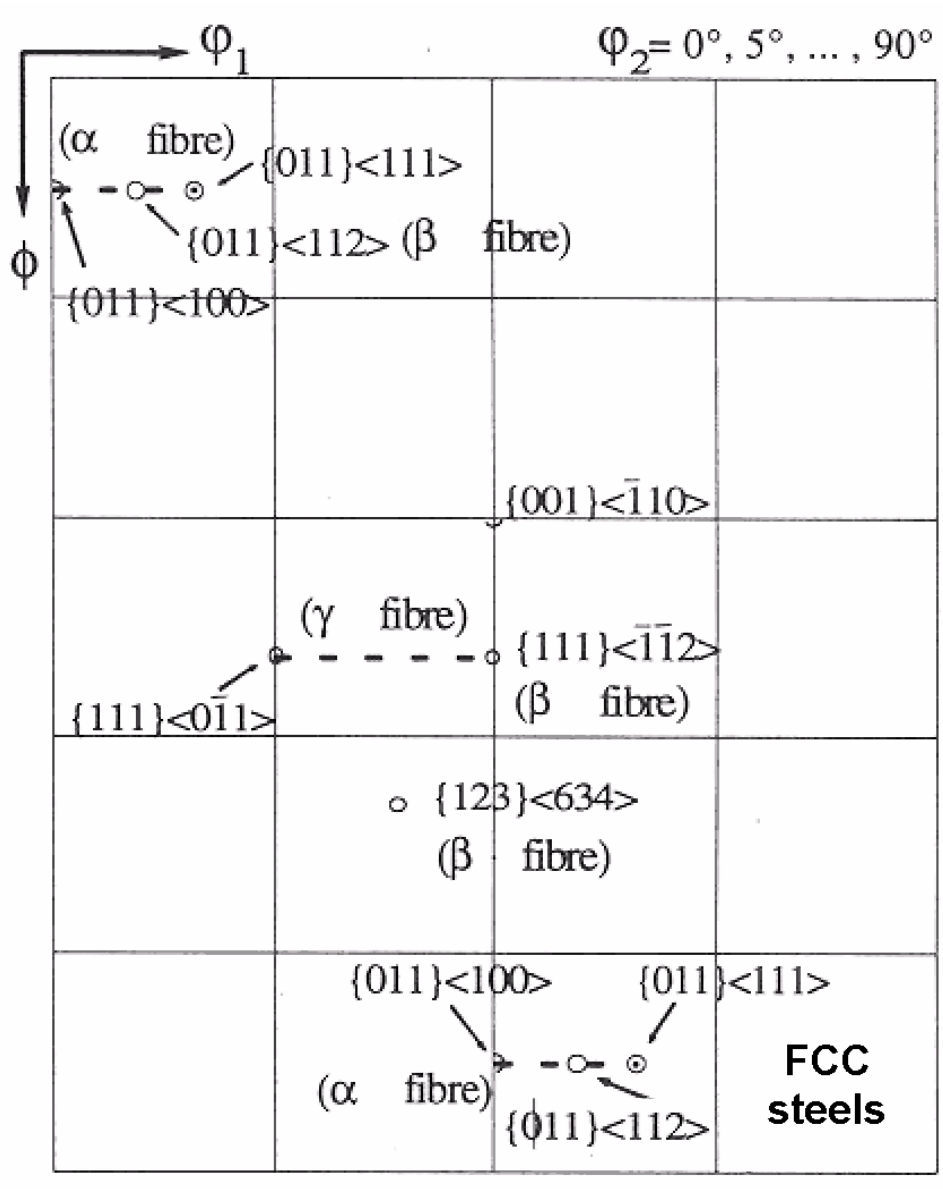

Figure 2: Some important fibers and texture components for FCC steels in sections through the reduced Euler space.

4 Basic texture classes for hot rolled and strip cast steels

4.1 Group (A) steels

The dominant common characteristic feature for hot rolled group (A) steels is that they do usually not build up strong starting textures or substantial texture gradients during hot rolling [4,7,9,10,13,18-27]. During hot rolling many ferritic steels with small alloy content undergo pronounced γ-α-transformation after forming during cooling. This process randomizes the hot band texture. The γ-α-transformation follows fundamental crystallographic rotation relationships as originally formulated by Nishiyama-Wassermann [28,29]. According to their work a {111} lattice plane and a <211> lattice vector in the austenite correspond to a {110} plane and a <110> vector in the martensite. Following Davies et al. [30] these transformation rules can be expressed in terms of a 95.3° rotation about a common <hkl> axis with h=-1+√2+√3, k=1+√2+√3 and l=√2. Ray and Jonas [6], Raabe [31,32], and Brückner et al. [33,34] observed these transformation relationships also in their experimental work. The multiplicity of possible transformations, when applied to each texture component of a hot rolled steel, entails an overall reduction of the texture sharpness after transformation. Variant selection mechanisms promoting only a limited set of transformations do usually not compensate for this multiplicity, i.e. most hot rolled group (A) steels reveal very weak textures.

Conventionally rolled low carbon and IF steels may undergo rather complete phase transformation at the end of hot rolling. For these steels the observed types of hot band textures, which are very important for the final product since they are inherited as starting textures to cold rolling, depend significantly on the details of the respective hot rolling strategy. Low carbon and IF steel sheets which are finished in the ferritic regime typically reveal some weak texture components which are characteristic of *cold* band textures at the end of hot rolling [35-39]. Using a *ferritic* hot rolling strategy means that at least the last or the last two hot rolling steps are carried out in the α phase region. This implies that the transformation takes place before the end of hot rolling. Steels which are finished in the ferritic regime do not only show residual rolling textures but also weak through-thickness and in-plane texture gradients after cooling, Figures 3a,b. Low carbon steels which are finished using an austenitic hot rolling strategy mostly reveal nearly random textures at the end of hot rolling.

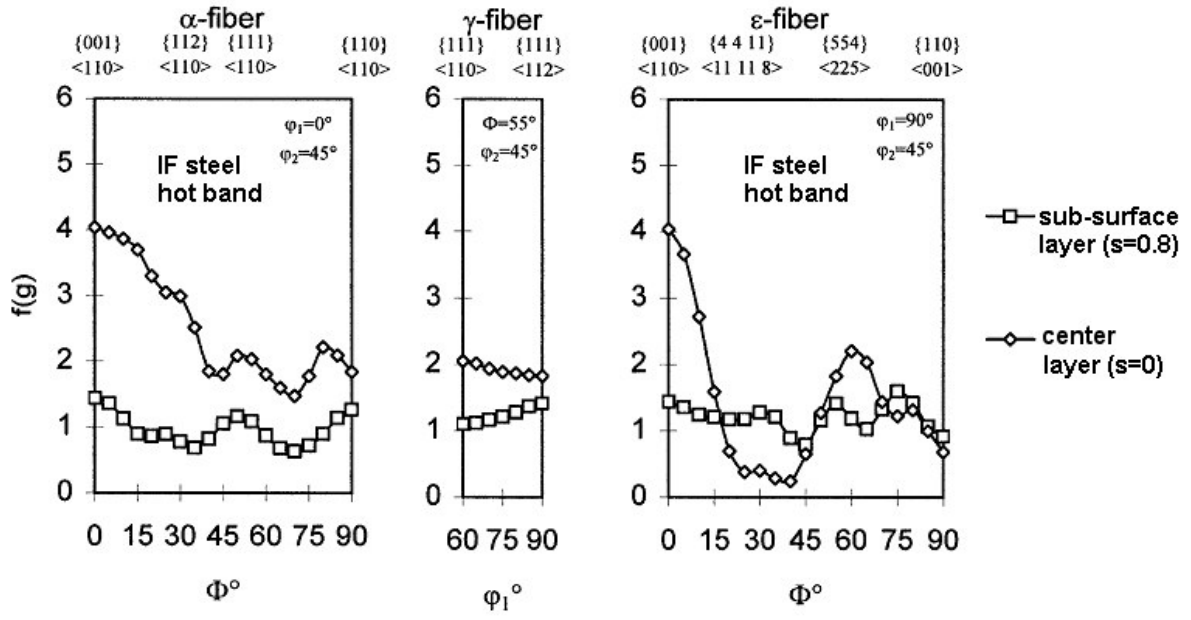

Figure 3a: Texture inhomogeneity of an hot rolled IF steel through the sheet thickness [35] (group A).

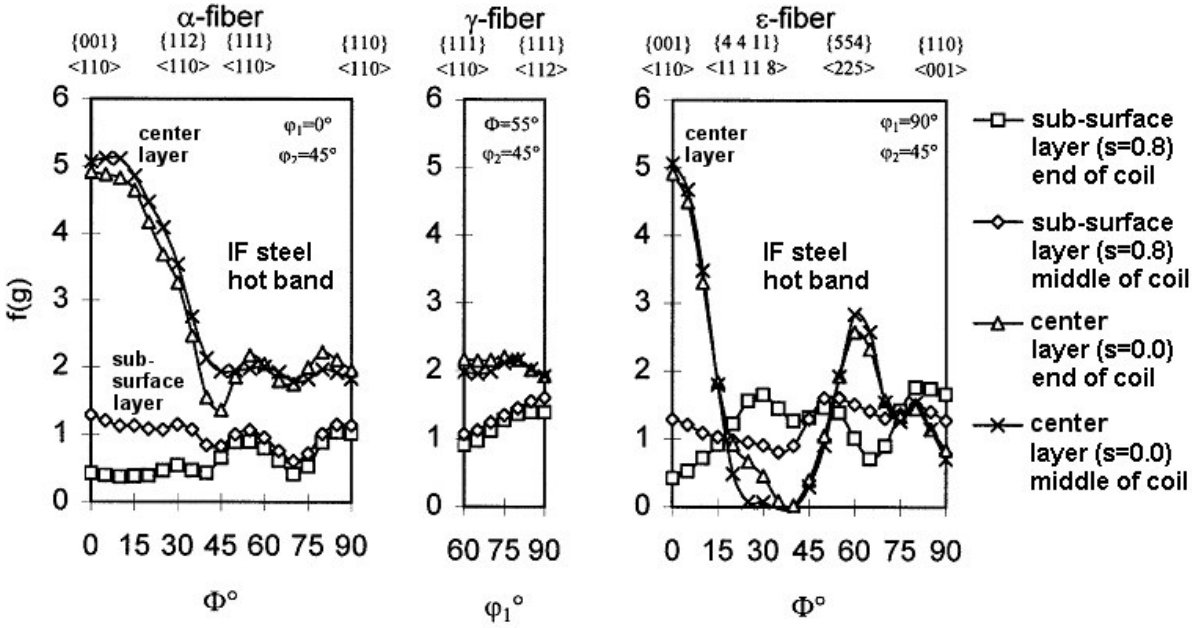

Figure 3b: Texture inhomogeneity of an IF steel in the sheet plane of a hot rolled coil [35] (group A).

Similar textures with random or weak cube-type fiber orientation distributions are observed in highly alloyed corrosion-resistant ferritic and austenitic stainless steels, low-carbon steels, and Si-steels when they are produced via thin strip casting, Figures 4,5 [12,31,40-47]. In this case corrosion-resistant stainless steels can be classified as group (A) materials. However, strip cast stainless steels typically reveal an inhomogeneous microstructure through the sheets thickness. The surface and near-center layers are often characterized by large, uniform blocks of dendrites. The layers close to the center show a more blocky and nearly equiaxed morphology. The mid-thickness layer of strip cast material often shows a globulitic grain structure. Nonstable austenitic grades can contain up to 20vol.% martensite in the center layers [31,47].

Both types of corrosion-resistant stainless steels (ferritic, austenitic) reveal a nearly random orientation distribution in all through thickness layers of the strip cast material. The observed texture gradients are in both types of alloys negligible when compared to the corresponding hot bands. The highest orientation density does usually not exceed a value of f(g)=4 times random. Strip casting textures are usually unequal on both sides of the sheet, i.e. the through-thickness texture is not symmetric with respect to the center layer, Figures 4,5.

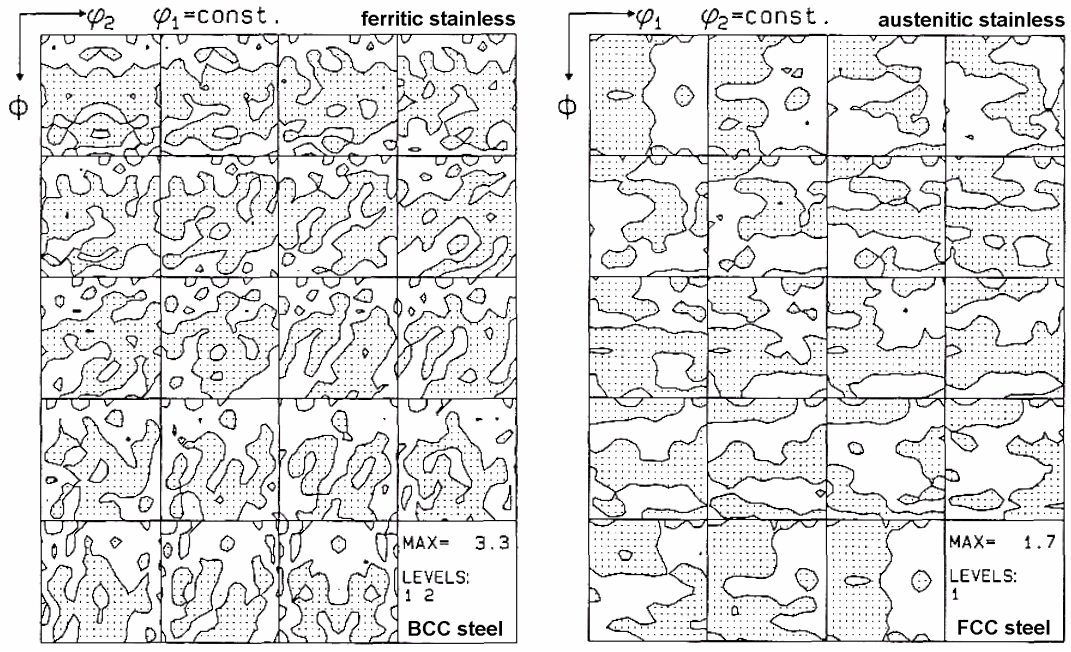

Figure 4: Example of the weak textures of a strip cast ferritic (left) and austenitic (right) stainless steels [12,47] (group A, center layers).

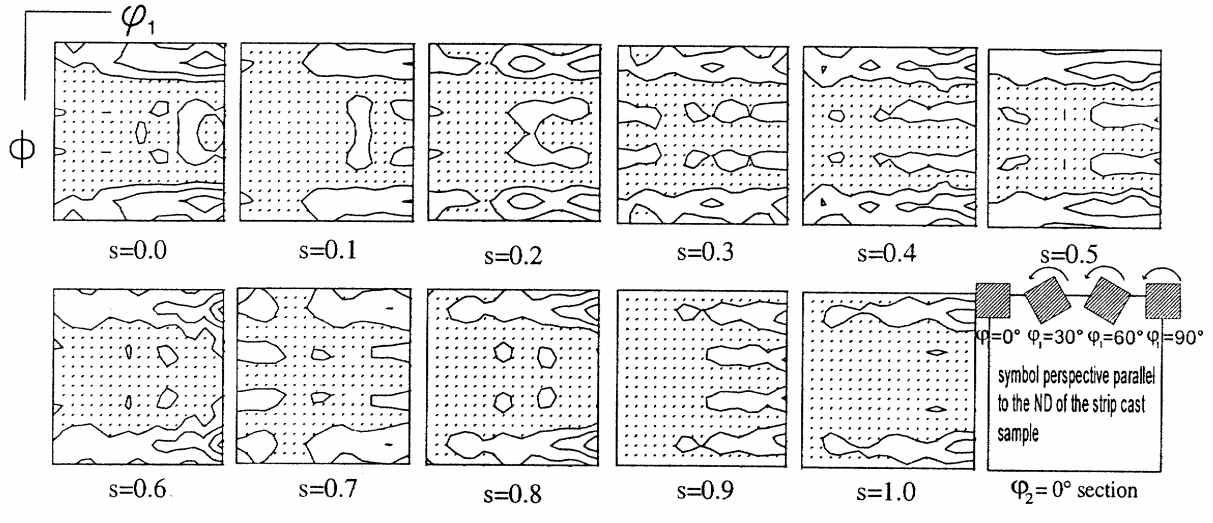

Figure 5: Example of the very weak through-thickness texture gradient of a strip cast austenitic stainless steel which is characterized by a weak fiber texture typical of solidification processes [12,47]. The iso-intensity lines are f(g)=0.5, 1, and 1.5 times random (group A).

4.2 Group (B) steels

Highly alloyed corrosion-resistant ferritic stainless steels (e.g. Fe-11wt.%Cr, Fe-17wt.%Cr) and most Si-steels reveal a smaller volume fraction of austenite during hot rolling [7,9-13,48,49]. Similar criteria apply for pure and weakly alloyed BCC refractory metals such as Ta, Mo, or Nb [13,50-55] which do not undergo any solid-state phase transformation during hot rolling. These materials have in common that they reveal strong *cold* rolling-type textures at the end of hot rolling due to their ferritic stability during hot rolling.

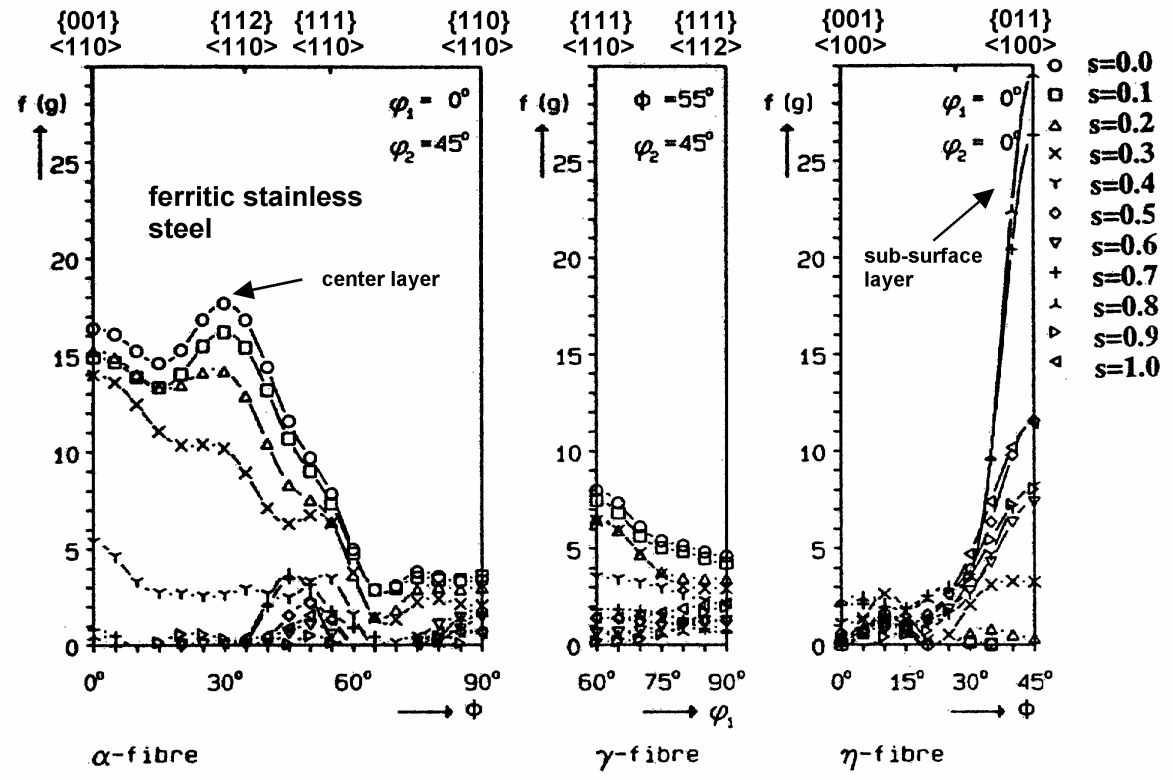

Figure 6: Example of the strong through-thickness texture gradient of an as hot rolled ferritic stainless steel [11] (group B). It is worth noting that the texture gradient in group (B) steels is much stronger than in group (A) low carbon or IF steels even when they were finished in the ferritic regime.

In contrast to the usually random or at least weak starting textures of the group (A) steels or of strip cast steels, group (B) materials are characterized by strong gradients in texture and microstructure through the sample thickness, Figures 6,7. Thoroughly investigated examples are Fe with 3wt.% Si and Fe with 10wt.%-16wt.% Cr [7,9-13,48,49]. In the center layer these materials show after hot rolling a flat and elongated grain morphology with a low fraction of recrystallized grains. At the surface they show a larger amount of recrystallized equiaxed grains. Concerning the textures they exhibit in the center layer a strong α-fiber and a weak γ-fiber. Close to the surface (s≈0.8) they typically reveal a completely different texture, namely, a strong ζ-fiber with pronounced orientations between {011}<112> and the Goss component, {011}<100>, accompanied by the ε-fiber with strong orientations between {112}<111> and {4 4 11}<11 11 8>.

These through- thickness texture profiles typically observed in hot rolled ferritic corrosion-resistant stainless steels can be explained in terms of the macroscopic gradients in shear and the temperature profiles occurring in these materials during hot rolling [56,57]. The center layers are essentially deformed by an plane strain deformation state. The grains in these layers typically assume an elongated pancake-type morphology. Cooling in the center layers is much slower when compared to the surface regimes. Both effects promote strong recovery instead of recrystallization in the center layers. Recovery is particularly important for the preservation of a strong α-fiber texture often with a maximum at the {001}<110> texture component [58]. This orientation is particularly prone to undergo recovery instead of recrystallization due to absence of in-grain orientation gradients [59,60]. The α-fiber texture in the center layers of the hot rolled sheet which is inherited and stabilized by cold rolling is also considered to be the main reason for the above mentioned ridging phenomenon especially in Fe-17%Cr alloys. It is assumed in this context that the clustered lateral distribution of certain texture components such as the main α-fiber components {001}<110>, {112}<110>, and {111}<110> in case of ferritic steels, can lead to an unfavorable topological arrangement of the out–of–plane shears which is referred to as ridging. Only a reduction of these components and their topological clustering in the hot band texture, a change of the deformation mode, or the randomization of the texture by phase transformation can eliminate the ridging phenomenon [61-64].

The appearance of rolling texture components in the center layers of hot rolled alloyed steels and related alloys can be explained in terms of the Relaxed Constraints Taylor theory (RC) [65-74]. The RC-model variants assume, in contrast to the full strain rate constraints assumption suggested originally by Taylor [75], that in the grains shear strains parallel to the rolling plane may occur, at low strains only in RD (lath- or C-model), at high strains additionally in TD (pancake- or SC-model). In addition to these geometrical aspects the influence of the various types of BCC slip systems, namely, 12 {110}<111>, 24 {110}<111> plus {112}<111>, or even 48 {110}<111>, {112}<111> plus {123}<111> slip systems, deserves attention when predicting BCC textures. Texture simulations on the basis of the 12 {110}<111> glide systems lead to results which are characterized by two isolated orientations {112}<110> and {111}<110> on the α-fiber and the evolution of the γ-fiber. Whereas for weak plane-strain rolling strains the maximum on the α-fiber is located close to {001}<110>, after 70% rolling this component is

shifted towards {112}<110>. Considering additionally the 12 {112}<111> glide systems with identical critical resolved shear stress (CRSS) as on the {110}<111> slip systems promotes the two main orientations {001}<110> and {111}<110> on the α-fiber and the development of a weak {111}<112> component on the γ-fiber. When taking into account additionally the 24 {123}<111> glide systems with identical CRSS the simulations yield a somewhat more uniformly shaped α-fiber. Recent variants of the Taylor model which take into account the interaction of the grains yield improved texture predictions [76,77].

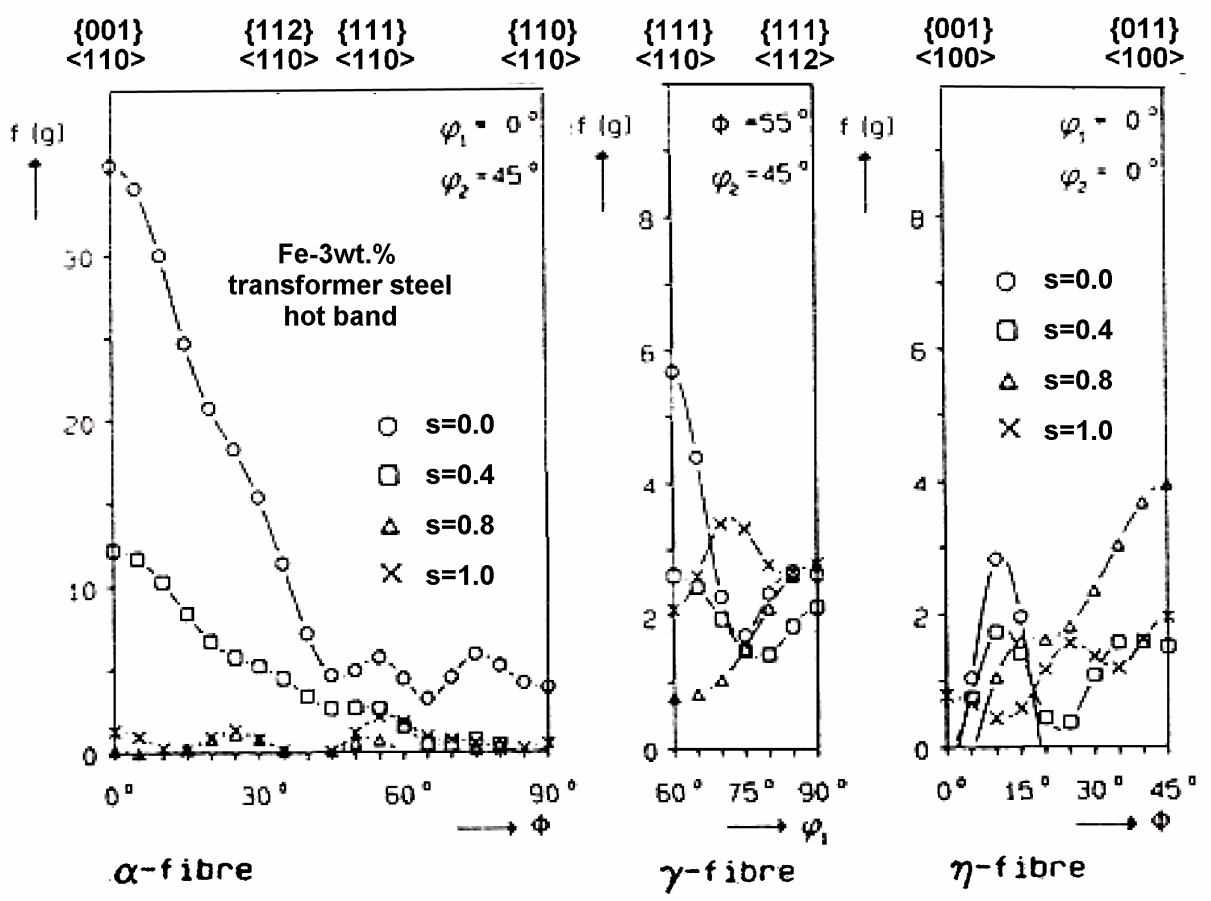

Figure 7: Example of the strong through-thickness texture gradient of an as hot rolled Fe-Si transformer steel [9] (group B).

The near-surface layers of hot formed sheets are characterized by a strong shear deformation and a large von Mises equivalent strain. The values of the orientation densities of the shear components {011}<100>, {110}<112>, and {4 4 11}<11 11 8> at the various depths correspond to the profile of the shear strain which results from the influence of the temperature on the flow stress and the through-thickness profile of the Zener Holomon parameter, as calculated by

Beynon et al. [56] and McLarren and Sellars [57]. Particularly the Goss orientation, {011}<100>, is well known to be stabilized by shear strain. The strong near-surface maximum of the Goss component in group (B) materials occurring at s=0.8 corresponds exactly to the ideal shear texture which is found in torsion experiments. The strong maximum of the von Mises equivalent strain in conjunction with strong shear components in the sub-surface layers of the hot band promotes local shear banding and recrystallization instead of recovery.

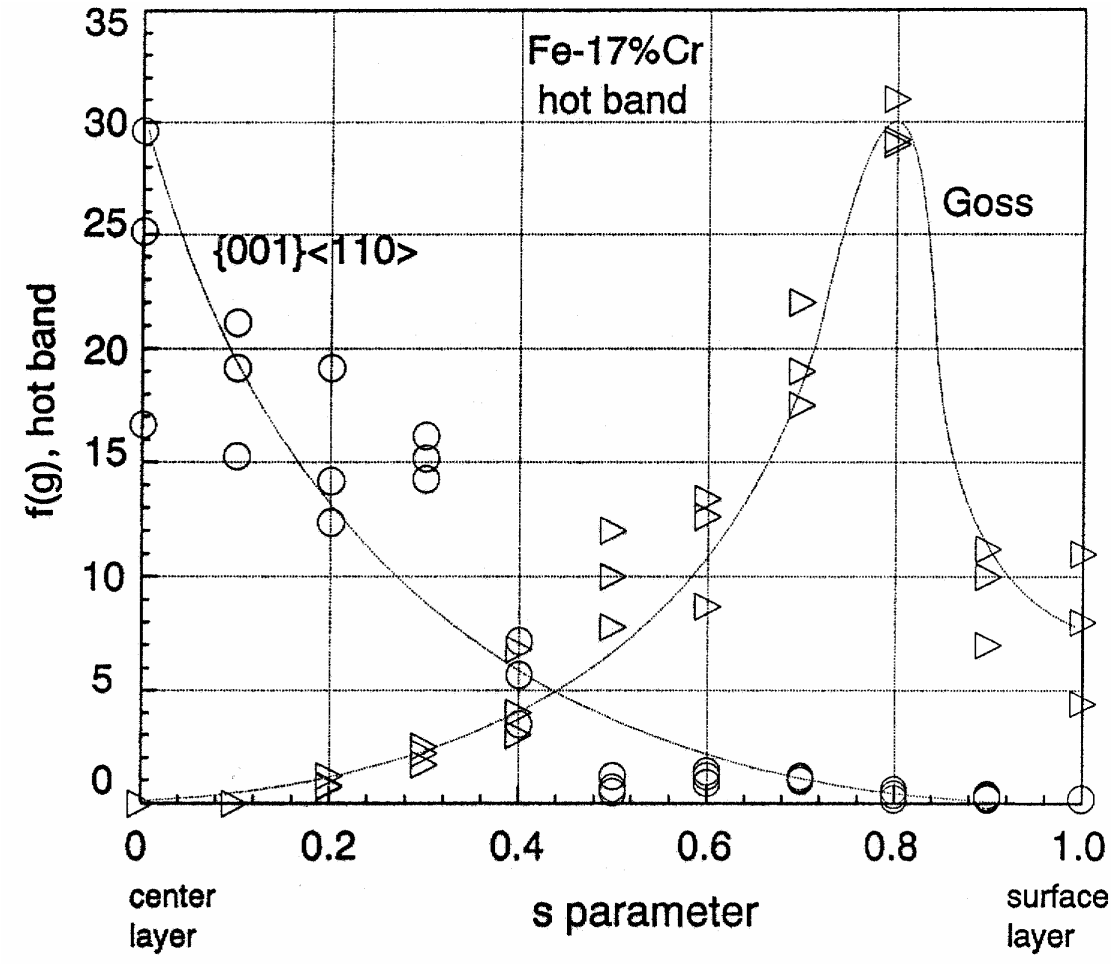

Figure 8: Example of the strong through-thickness texture gradient of a ferritic stainless steel in terms of a plane-strain texture component ({001}<110>) and of a shear texture component (Goss) (group B).

High melting BCC refractory metals also reveal inhomogeneous through-thickness hot rolling textures. This observation is usually attributed to the complicated hot rolling schemes usually employed for these materials. They are often processed by a set of hot rolling steps and several intermediate off-line annealing treatments which are required to soften the sheets prior to further rolling. During these intermediate heat treatments BCC refractory metals often undergo recovery instead of primary recrystallization. However, recrystallization and recovery are strongly orientation dependent in all BCC materials entailing sometimes highly inhomogeneous microstructures and textures even in the same through-thickness layer.

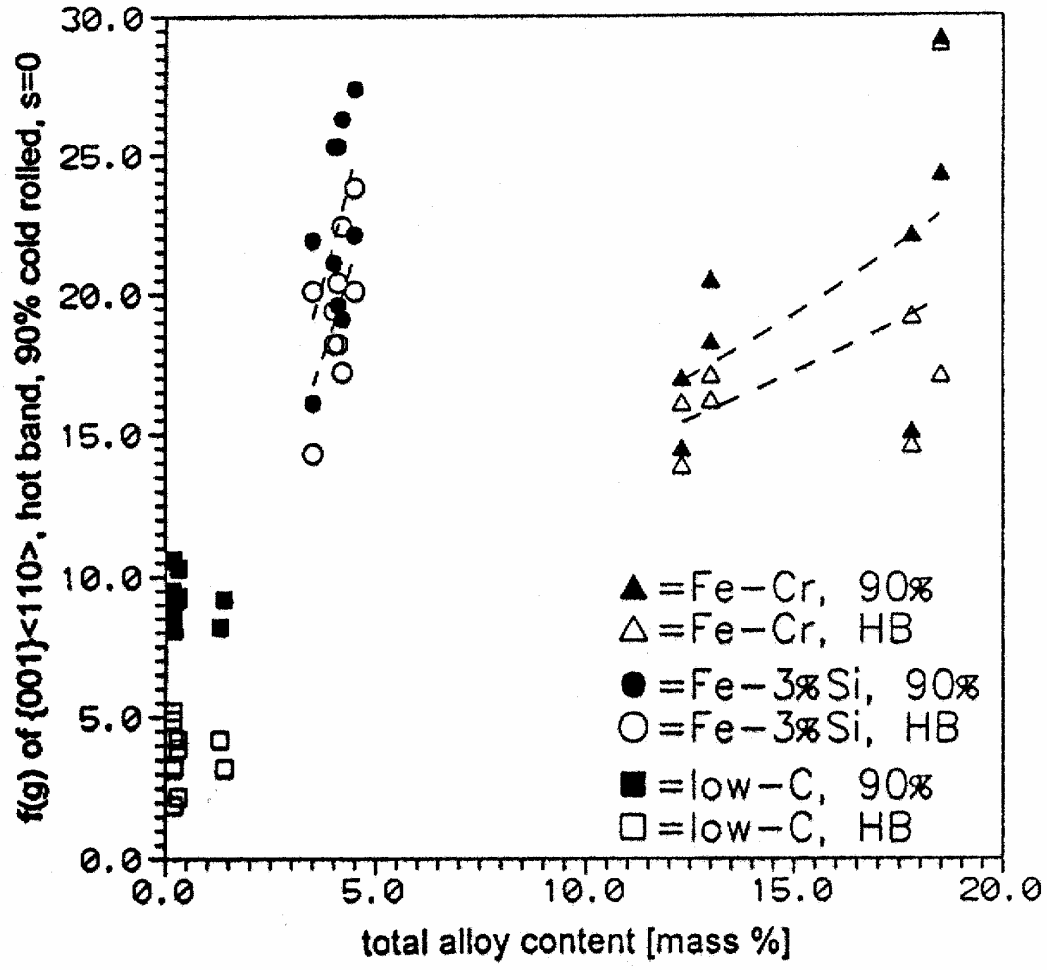

Figure 9: Example of the influence of the starting textures prior to cold rolling as inherited from the hot band on the evolution of the cold rolling texture for different alloys (group B). (HB=hot band, 90%= 90% cold rolled, all data are taken from the center layer).

As outlined above the occurrence of a strong recovered {001}<110> texture component in the center layer of hot rolled sheets and of a strong shear texture containing for instance the Goss component close to the surface is characteristic of most hot rolled group (B) materials. The maximum of the shear texture components is in hot rolled ferritic stainless steels frequently located at s=0.7-0.8. When the texture profile is inspected with a local through-thickness resolution of $\Delta s=0.1$ as for instance shown in Figure 6, it can be seen that between the center and the surface layers a continuous decrease of the plane-strain type rolling texture and the steady increase of the typical shear texture components represent characteristic features of these steels. The resulting profile of the orientation density of the Goss component through various depths, here showing data from various steels with 17% Cr content, is depicted in Figure 8. The occurrence of this type of texture profile within a hot rolled stainless steel band is well known from various ferritic alloys containing 11% Cr, 17% Cr or 3.4 % Si, respectively [7,9-13,48,49]. Figure 9 shows that with increasing alloy content especially of Cr and Si, i.e. with decreasing volume fraction of phase transformation during hot rolling, the intensity of the orientation density of the mid-thickness plane-strain component {001}<110> is enhanced.

4.3 Group (C) steels

Austenitic stainless steels and duplex stainless steels show in part deformation induced phase transformation during hot rolling. However, the volume fraction affected by such transformation is usually much below that in low carbon and IF steels. Therefore, most steels of group C usually have non-random textures after hot rolling. Most steels in this group typically deform as FCC materials without much transformation during cooling after hot rolling. The stacking fault energy of the FCC phase is usually similar to that of 70/30 brass, i.e. the materials pertaining to group (C) principally have a smaller tendency to recover and instead a larger tendency to recrystallize when compared to ferritic stainless steels. The hot band rolling textures of stable austenites and brass are, therefore, also similar.

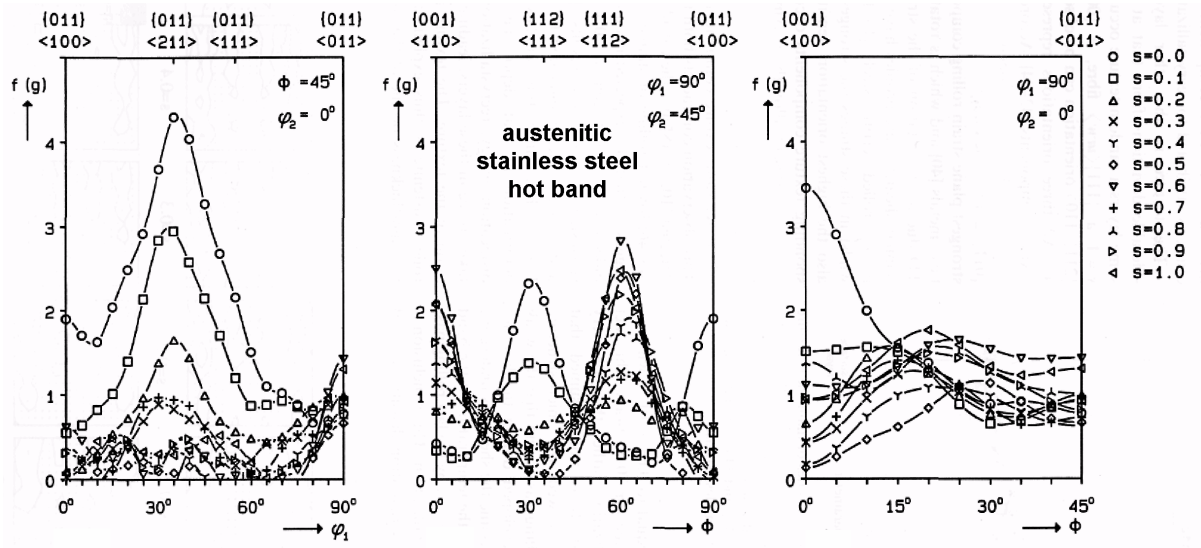

Figure 10: Example of the through-thickness texture gradient of an as hot rolled austenitic stainless steel [31] (group C).

Austenitic hot band sheets typically reveal an inhomogeneous texture profile through the thickness, Figure 10. Close to the center layer, i.e. at s=0.0 and s=0.1 the orientation distribution is characterized by a weak β-fiber with a maximum at {011}<211>, accompanied by the appearance of a weak cube component {001}<100>. In the layer s=0.2 these orientations are often decreased and a nearly random orientation distribution is detected. Close to s=0.5 and s=0.6 a texture transition takes place. Three new orientations, namely, a weak {001}<110> component, a γ-fiber, and a strong {112}<110> orientation, which corresponds to the 30° about TD rotated rolling component {110}<112>, are usually developed. In the sub-surface layers at s=0.7 and s=0.8 the texture is often again close to random. At the surface (s=1.0) a similar texture as in layer s=0.6 is developed. In order to describe the through-thickness texture profile of the hot rolled austenitic stainless steel the three shear components which show a maximum orientation density close to s=0.6 can be chosen as indicators for the shear profile as shown in Figure 11. It is revealed that the orientation density of all three components shows a similar course in various depths. Close to the center layer both orientations are very weak and continuously increase up to the layer s=0.6. Between s=0.6 and s=0.9 a decrease and at the surface again an increase of the three shear components can be seen. This course represents the main contrast to ferritic hot band materials where the shear components reveal a maximum at s=0.8 and not at s=0.6 or s=1.0, respectively.

According to experimental results by Goodman and Hu [78], Donadille et al. [79], and Raabe [31] as well as Taylor-based simulations by Hirsch and Lücke [80] the observed β-fiber at s=0 are typical rolling texture components which results from plane-strain deformation of FCC polycrystals. However, in the present austenitic hot band the maximum orientation density is lower than after cold rolling of comparable alloys, Figure 10. Since complete recrystallization during or after hot rolling would have completely removed the detected rolling texture at s=0, this result suggests strong recovery during hot rolling. Such argumentation, however, is often in contradiction to the hot band microstructures of austenitic stainless steels, which typically consist of equiaxed instead of elongated grains. Also, the low stacking fault energy of austenitic stainless steels which is of the order of $20 \cdot 10^{-3}$ J/m^2 suggests a strong tendency for recrystallization instead for recovery. It is, therefore, possible that recrystallization has occurred already at the beginning of hot rolling and that the weak β-fiber texture was developed during the last rolling passes, i.e. after considerable cooling of the sheet where the temperature of the band and the stored energy imposed by the last rolling pass were too low for an overall recrystallization. This conclusion is in good agreement with the observed low orientation density, because recovery of rolled material would have led to a much stronger texture maximum. Owing to the low stacking fault energy of austenitic stainless steels the occurrence of the cube orientation in the center layer of the austenitic hot band can be interpreted in terms of recrystallization.

The textures in the other layers considerably differ from that at s=0. Some layers reveal a nearly random texture, for instance s=0.6 and s=1. Other layers show a γ-fiber texture which is accompanied by a {001}<110> and a {112}<110> orientation. The three texture components are well known from other inhomogeneously rolled FCC materials such as from Al and represent typical shear orientations [31]. The {112}<110> component results from the {011}<211> orientation, which represents the strongest ideal plane strain rolling component in FCC metals with a low stacking fault energy and which has been rotated 30° about the TD due to the rotation of the strain state.

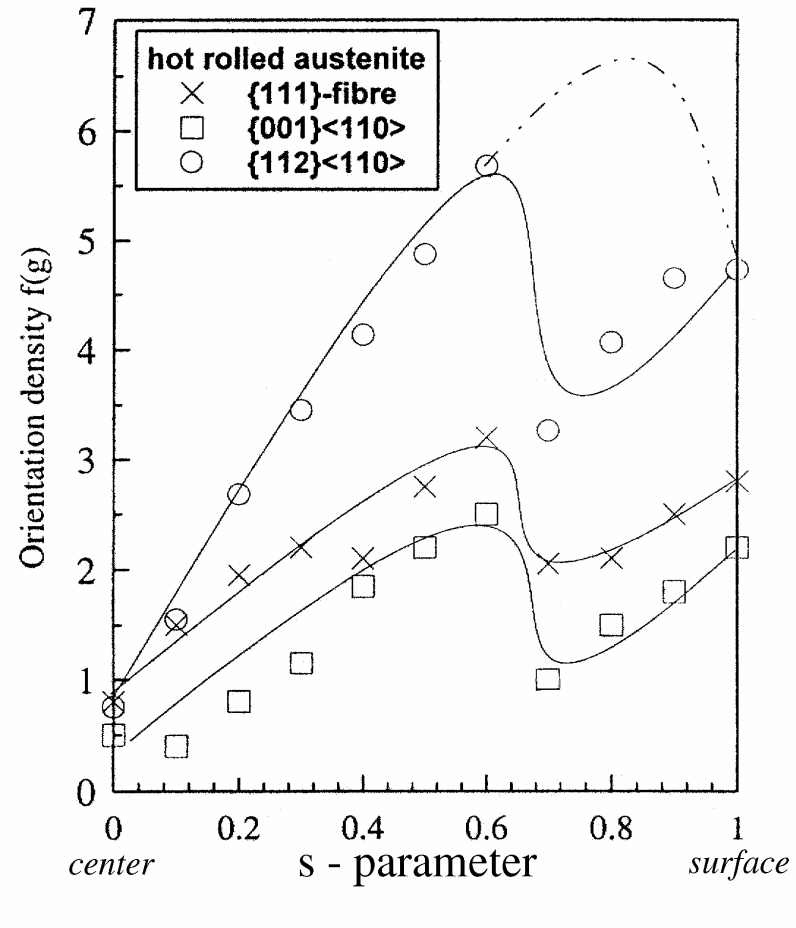

Figure 11: Example of the through-thickness texture gradient of a hot rolled austenitic stainless steel in terms of the gradient of some shear components [31] (group C).

The through-thickness profile of the austenitic shear components thus basically corresponds to the profile observed for the shear orientations of the ferritic hot bands. However, while in the ferritic steel the highest orientation densities of the shear components occur at s=0.7-0.8, the austenitic hot band has a split maximum of the shear texture with one peak at s=0.6 and a second one at s=1. The layers s=0.7 and 0.8 even show a local minimum, Figure 11. In order to explain this deviation of the austenitic texture profile it is assumed that the maximum of the shear was truly positioned within the range s=0.7-s=0.8 as suggested by macroscopic considerations (schematically indicated by the dotted line in Figure 11). But since this implies larger local von Mises strain, i.e. also a higher stored dislocation energy, it is assumed that in these layers recrystallization could take place more easily, leading to the randomization of the texture.

CONCLUSIONS

The present work gave an overview of the evolution of hot rolling textures of steels. Textures arising from thin strip casting were also included in the review. The data show that the textures of steel hot bands can be divided into three groups. The first group comprises pure Fe, weakly bonded B2 and $D0_3$ structured intermetallics, as well as closely related alloys such as ferritic low carbon and microalloyed interstitial free steels. The second group includes highly alloyed corrosion-resistant ferritic stainless and Fe-Si transformer steels. Typical examples are steels with about 10 wt.%-17 wt.% Cr, with about 3 wt.% Si, as well as body centered cubic transition metals such as Ta, Mo, and Nb which do not undergo a phase transformation during hot rolling. The third group comprises stable and instable austenitic stainless steels for instance on the basis of larger amounts of Cr and Ni or on Mn as well as duplex stainless steels. Most $L1_2$ structured intermetallic alloys can also be assigned to this group. The suggested classification scheme was discussed in terms of different processing parameters, thermodynamic boundary conditions, microstructural parameters, and crystallographic aspects. The main details of the overview are:

- The main difference between group (A) and group (B) steels (both BCC) essentially proceeds from their different thermodynamic behavior during hot rolling. Group (B) materials are essentially rolled in the ferritic regime.
- Group (C) steels are essentially hot rolled in the austenitic regime leading to non-random austenite textures and pronounced texture gradients through the sheet thickness.
- Group (C) steels have a larger tendency to undergo recrystallization during hot rolling when compared to group (A) and group (B) steels which reveal stronger recovery effects. This effect is due to the small stacking fault energy of the austenitic phase.
- Group (B) materials have a strong and group (A) materials have nearly no texture gradient through the thickness of the hot band when finished in the austenitic regime. Group (A) steels can show weak textures and texture gradients when finished in the ferritic regime. Group (C) steels do also show texture gradients, but they are usually weaker than in group (B) hot bands. This difference is due to the fact that group (B) steels have a larger tendency to recovery rather than to recrystallize such as group (C) steels owing to the differences in stacking fault energy between the BCC and FCC phase.
- Hot bands of group (B) steels reveal a shear texture with Goss at the surface and a cold-rolling-type of texture with α-fiber in the center layer. Group (A) metals show a nearly random initial texture when finished in the austenitic regime.
- The increase of the Cr or Si content leads to the increase of the initial α-fiber in the center layer of group (B) alloys.
- Strip casting leads for all steels to nearly random textures or to very weak fiber textures.

REFERENCES

1. H.J. Bunge, Texture Analysis in Materials Science, 1982, Butterworths, London.
2. H.J.Bunge, Z. Metallkunde 56, 872 (1965).
3. G. Wassermann, J. Grewen: "Texturen metallischer Werkstoffe", Springer Verlag, Berlin Göttingen, Heidelberg, 2nd ed. (1962) (in German).
4. M. Hölscher, D.Raabe and K.Lücke, Steel res. 62, 567, (1991).
5. M. Hölscher, D. Raabe, K. Lücke: Acta metall. 42 (1994) 879–886
6. R. Ray and J. Jonas.; Int. Mat. Rev. Vol.35, p.1 (1990)
7. D. Raabe, K. Lücke: Materials Science Forum 157–162 (1994) 1469–1474.
8. D. Raabe, H. Krause, A. D. Rollett, A. Teicher: Proceedings of the 12th International Conference on Textures of Materials ICOTOM 12, Aug. 9–13, 1999, Montreal, Canada, eds.: Jerzy A. Szpunar, NRC Research Press, National Research Council of Canada, Building M–55, Ottawa, ON K1A 0R6, Canada, 1999, Volume 2, 1015–1024.
9. D. Raabe, K. Lücke: Scripta Metall. 26 (1992) 1221–1226
10. D. Raabe, K. Lücke: Scripta Metall. 27 (1992) 1533–1538
11. D. Raabe, K. Lücke: Materials Science and Technology 9 (1993) 302–312
12. D. Raabe: Materials Science and Technology 11 (1995) 461–468
13. D. Raabe, Textures of body centred–cubic transition metals, Ph. D. Dissertation, RWTH Aachen, 1992 (in German).
14. L.G.Schulz, Journ. Appl. Phys. 20, 1030 (1949).
15. M. Dahms, Text. and Microstr., 19, 169 (1992).
16. M. Dahms and H. J. Bunge; J. Appl. Cryst. Vol.22, p.439 (1989)
17. D. Raabe: Textures and Microstructures 23 (1995) 115–129
18. F.Haessner, D.Mayer-Rosa: Z.Metallkunde 58 (1967) H1 12-19.
19. I.L.Dillamore, W.T.Roberts, Acta Metall. 12, 281 (1964).
20. I.L. Dillamore and H. Katoh, Metal. Sci. 8, 21 (1974).
21. C. Klinkenberg, D. Raabe and K. Lücke, Steel Res. 63, 227 (1992).
22. C. Därmann, Text. and Microstruc. 14-18, 819 (1991).
23. W.B. Hutchinson; Int. Mat. Rev. Vol.29, p.25 (1984)
24. K. Ushioda, W. B. Hutchinson, J. Agren and U. von Schlippenbach; Mat. Sc. and Techn. Vol.2, p.807 (1986)
25. W. B. Hutchinson, Philosophical transactions. 1999 v 357 n 1756 , page 1471, Deformation microstructures and textures in steels.
26. C. Därmann, S. Mishra and K. Lücke, Acta Met. 32, 2185 (1984).
27. U.v. Schlippenbach, F. Emren and K. Lücke, Acta Met. 34, 1289 (1986).
28. Z. Nishiyama, Sci. Rep. Inst., Tohoku Univ. 23, 638 (1934/1935).
29. G. Wassermann, Archiv Eisenhüttenwesen 16, 647 (1933).
30. G. J. Davies, J. S. Kallend and P. P. Morris, Acta Metall. 24, 159 (1976).
31. D. Raabe: Acta Materialia 45 (1997) 1137–1151
32. D. Raabe: Journal of Materials Science 30 (1995) 47–52
33. G. Brückner, J. Pospiech, L. Seidl, G. Gottstein ; Scripta mater. 44 (2001) 2635-2640
34. G. Brückner, G. Gottstein ; ISIJ Intern. 41 (2001), 468-477
35. P. Juntunen, D. Raabe, P. Karjalainen, T. Kopio, G. Bolle: Metallurgical and Materials Transactions A, 32 (2001) 1989-1995
36. Y.B. Park, D.N. Lee, G. Gottstein ; Acta Mater. 44 (1997) 3421-3427
37. Y.B. Park, D.N. Lee, G. Gottstein ; Proc. ICOTOM 11 "Textures of Materials", Xi'an, China (Hrsg. Z. Liang, L. Zuo, Y. Chu) Intern. Academic Publ. Vol.I (1996) 324-329

38. D.O. Wilshynsky, G. Krauss, D.K. Matlock, International Symposium on Intertitial Free Steel Sheet: Processing, Fabrication and Properties, Ed. L.E. Collins and D.L. Baragar, canadian Inst. of Mining, Metallurgy and Petroleum, 1991, 69-80.
39. L. Kestens, J. J. Jonas, ISIJ international, Vol. 37, Nr. 8 (1997) Seiten 807–832, Modelling texture change during the static recrystallization of a cold rolled and annealed ultra low carbon steel previously warm rolled in the ferrite region
40. D. Raabe, M. Hölscher, M. Dubke, H. Pfeifer, H. Hanke and K. Lücke, Steel Res. 64, 359 (1993).
41. D. Raabe, M. Hölscher, M. Dubke, K. Lücke: Proceedings of International Conference on Strip Casting, Hot and Cold Working of Stainless Steels, Quebec, Canada, 1993, ed.N.D. Ryan, A.J. Brown, H.J. McQueen, The Metallurgical Society of the Candian Institute of Materials (CIM) 3−17.
42. D. Raabe, K. Lücke: Proceedings of International Conference on Strip Casting, Hot and Cold Working of Stainless Steels, Quebec, Canada, 1993, ed.N.D. Ryan, A.J. Brown, H.J. McQueen, The Metallurgical Society of the Candian Institute of Materials (CIM) 221−235.
43. D. Raabe, M. Hölscher, M. Dubke, F. Reher, K. Lücke: Materials Science Forum 157−162 (1994) 1039−1044.
44. D. Raabe, H. Krause: Proceedings of the 11th International Conference on Textures of Materials ICOTOM 11, Sept. 16-20, 1996, Xi'an, China, eds.: Z. Liang, L. Zuo, Y. Chu, International Academic Publishers, 137 Chaonei Dajie, Beijing 100010, China, ISBN 7-80003-376-7/TG.26, Vol. 2, 854−859.
45. D. Raabe, H. Krause, A. D. Rollett, A. Teicher: Proceedings of the 12th International Conference on Textures of Materials ICOTOM 12, Aug. 9−13, 1999, Montreal, Canada, eds.: Jerzy A. Szpunar, NRC Research Press, National Research Council of Canada, Building M–55, Ottawa, ON K1A 0R6, Canada, 1999, Volume 2, 1015−1024.
46. D. Raabe, M. Hölscher, F. Reher, K. Lücke: Scripta Metall. 29 (1993) 113−116
47. D. Raabe: Metallurgical and Materials Transactions A 26A April (1995) 991−998
48. M. Matsuo: ISIJ int., 29, 809 (1989).
49. L. Seidel, M. Hölscher and K. Lücke, Text. and Microstr. 11, 171, (1989)
50. D. Raabe, G. Schlenkert, H. Weisshaupt, K. Lücke: Materials Science and Technology 10 (1994) 229−305
51. D. Raabe, K. Lücke, G. Gottstein: Journal de Physique IV, colloque C7, supplément au Journal de Physique III 3 (1993) 523−526.
52. D. Raabe, B. Mülders, K. Lücke, G. Gottstein: Materials Science Forum 157−162 (1994) 841−846.
53. D. Raabe, G. Gottstein: Journal de Physique IV, colloque C7, supplément au Journal de Physique III 3 (1993) 1727−1729.
54. D. Raabe, K. Lücke: Materials Science Forum 157−162 (1994) 597−610.
55. F. Heringhaus, U. Hangen, D. Raabe, G. Gottstein: Materials Science Forum 157−162 (1994) 709−714.
56. J. H. Beynon, A. R. S. Ponter and C. M. Sellars, Proc. Model. of Met. Forming., Kluwer Acad. Publ., 321 (1988).
57. A. J. McLaren and C. M. Sellars, Mater. Scien. and Techn. 8, 1090 (1992).
58. D. Raabe: Steel Research 66 (1995) 222−229
59. D. Raabe: physica status solidi (b) 181 (1994) 291−299
60. D. Raabe, Z. Zhao, S.–J. Park, F. Roters: Acta Materialia 50 (2002) 421–440
61. K Bethke, M. Hölscher, and K Lücke, Mater. Sci. For., vol. 157-162, (1994) 1137.

62. N. J. Wittridge and R. D. Knutsen, 1996. Materials Characterization 37:31-37.
63. R. D. Knutsen and N. J. Wittridge 1996. Proceedings of International Conference, Minerals and Materials '96, SAIMM, Somerset West, South Africa:II,632-640.
64. N. J. Wittridge and R. D. Knutsen, Mat. Sc. Engin. 1999, A269, 205.
65. U. F. Kocks and H. Chandra, Acta Metall. 30, 695 (1982).
66. E. Aernoudt, Proc. 5th Int. Conf. on Tex. of Mat. ICOTOM 5, ed. G. Gottstein and K. Lücke, Springer Verlag, 45 (1978).
67. R. J.Asaro, Acta Metall. 27, 445 (1979).
68. H. Honneff and H. Mecking, Proc. 5th Int. Conf. on Tex. of Mat. ICOTOM 5, ed. G. Gottstein and K. Lücke, Springer Verlag 265 (1978).
69. H. Honneff and H. Mecking, Proc. 6th Int. Conf. on Tex. of Mat. ICOTOM 6, ed. S. Nagashima, Iron and Steel Inst. of Japan 347 (1981).
70. J. L. Raphanel and P. van Houtte, Acta Metall. 33, 1481 (1985).
71. U. F. Kocks, C. Tomé, H.-R. Wenk, 1997. Texture and Anisotropy. Preferred Orientations in Polycrystals and Their Effect on Material Properties. Cambridge University Press, Cambridge, England.
72. D. Raabe: Materials Science and Technology 11 (1995) 455–460
73. D. Raabe: Acta metall. 44 (1996) 937–951
74. D. Raabe, J. Keichel, G. Gottstein: Acta Materialia 45 (1997) 2839–2849
75. G.I. Taylor, Journ. Inst. Met., 62, 307, (1938).
76. P. Van Houtte, L. Delannay and I. Samajdar, Textures and Microstructures, 31 (1999) 109-149.
77. L. S. Tóth, A. Molinari and D. Raabe, Metallurgical and Materials Transactions A, Volume 28A, Issue 11, November 1997, Pages 2343-2351
78. S. R. Goodman and H. Hu, Trans. AIME 230, 1413 (1964).
79. C. Donadille, R. Valle, P. Dervin and R. Penelle, Acta Met. 37, 1547 (1989).
80. J. Hirsch and K. Lücke, Acta Met. 36, 2863 (1988).